Rev.Adv.Mater.Sci. 5 (2003) 24-33

NANOSTRUCTURED BULK SOLIDS BY FIELD ACTIVATED SINTERING

J. R. Groza[1] and A. Zavaliangos[2]

[1]Chemical Engineering and Materials Science Department, University of California at Davis, One Shields Ave, Davis, CA 95616, USA
[2]Department of Materials Engineering, Drexel University, 32nd Chestnut Str., Philadelphia, PA 19104, USA

Received: June 23, 2003

Abstract. Field activated sintering is a novel processing technique with a high potential to process bulk nanomaterials with good interparticle bonding. The external field application is capable to induce fast densification and reasonable control of grain growth during sintering of nanocrystalline powders. The process has been applied for the densification of a variety of materials, electrically conductive, semiconductors or insulators.
This presentation will overview examples of field sintered nanomaterials and focus on studies of electrical field effects in sintering. The main mechanisms involved during electrical field densification and the interplay between the applied electrical current and densifying materials during field assisted sintering (electrical discharge, constriction resistance, current uniformity, heating rate and pressure effects) will be addressed.

1. INTRODUCTION

Nano – science and technology have been areas of intense fundamental and practical interest in the last decades. Processing and manufacturing of nanomaterials must capitalize on the most recent developments to keep pace with the new nano-science discoveries. In this context, **field assisted sintering techniques (FAST)** have emerged as novel processes to produce sintered parts via application of an external electrical current. The current application shortens the densification time, thereby making this process a good candidate for sintering nanostructured materials.

The electrical field activation has been pioneered by Taylor, who used resistance heating for hot pressing cemented carbides in 1933 [1]. In late 50's, resistance sintering under pressure was applied to metal powders by Lenel using equipment similar to spot welding [2]. Presently, resistive hot pressing is commonly used and consists of a low-voltage (5-40 V), high-amperage (up to 25 kA) current passing through the powders with a simultaneous pressure application. The main difference between FAST and hot pressing is the simultaneous application of a pulsed current in the former, which generates electrical discharges [3]. The electrical discharges per se do not densify powders and, therefore, additional energy is required to increase the final density. This extra energy may be mechanical, as an applied pressure, and thermal by generating higher temperatures than that created by electrical discharge.

Electrical current activation has been applied in the plasma assisted sintering (PAS) process developed in Japan in the 60's, followed by the presently largely used spark plasma sintering (SPS) [3]. Field sintering techniques are also known as instrumented pulse electro-discharge consolidation, pulsed electric current sintering, resistance/spark sintering under pressure, pulsed electrical discharge with pressure application, high energy high rate processing or pressure plasma sintering. All these methods are essentially identical in the application of a pulsed

Corresponding author: J.R. Groza, e-mail: jrgroza@ucdavis.edu

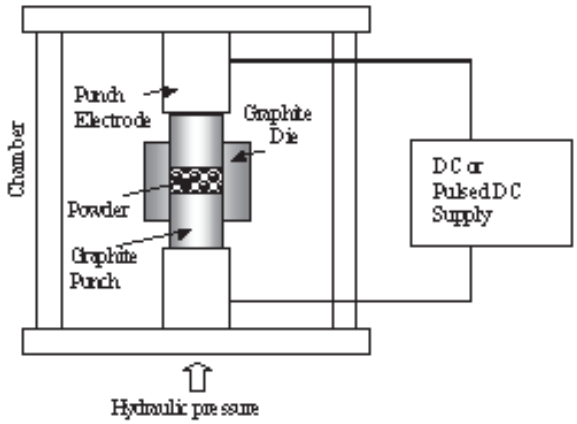

Fig. 1. Schematic of FAST process.

discharge and subsequent or simultaneous resistance sintering. The pulsed electro-discharge stage may be built-in as an added option for powder activation in other non-field sintering techniques, such as the piston-cylinder high pressure method [4]. These techniques are different from other electrical field assisted sintering methods such as electrodischarge compaction (EDC) [5]. In the latter, the electrical energy is suddenly released by discharging a capacitor bank through a powder compact. The discharge period is less than 100 μs at a high amperage current (~ 10 kA). This presentation will address only pulsed electrical discharge activated pressure sintering that will generally be called "field activated sintering technique" (FAST).

A schematic of the FAST process is shown in Fig. 1. The equipment consists of a mechanical device capable of uniaxial pressure application and electrical components to apply the pulsed and steady DC current. The loose powders are directly loaded into a punch and die unit without any additives. Graphite die and punches are commonly used. This limits the pressure levels to low values, generally < 100 MPa, although high pressure graphite may also be available. The pressure may be constant throughout the sintering cycle or changed in different densification stages. The graphite confinement provides a reducing component to the sintering environment. The machines are equipped with chambers for vacuum or controlled environment. A typical pulse discharge is achieved by the application of a low voltage (~30 V) and ~1000 A current. The duration of each pulse may be varied between 1 to 300 ms and on and off pulses may have different durations. The pulses may be applied throughout the whole sintering cycle, such as in SPS, or

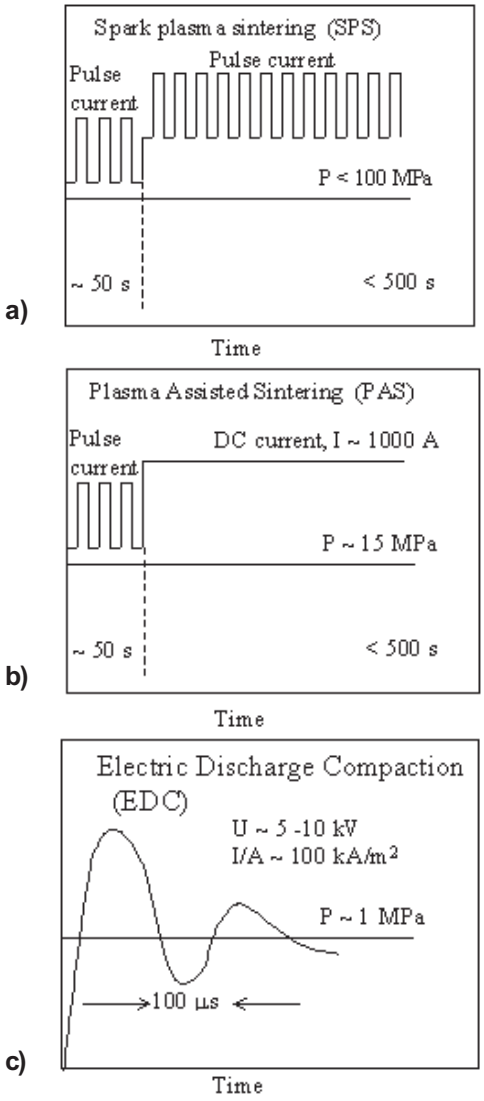

Fig. 2. Schematic of pulsed field application in SPS, PAS and EDC techniques.

only prior to the application of a steady DC current, such as in PAS (Fig. 1 a and b). Generally, the wave forms are square, but sinusoidal, seesaw or continuous may be also applied. The powders are mainly heated due to the Joule effect. While this effect heats directly the conductive powders, the non-conductive powders are heated by heat transfer from the Joule heated die and plungers.

2. FAST SINTERING OF NANOSIZE POWDERS

The pulsed current promotes electrical discharges at powder particle surfaces, thus activating them for subsequent bonding. The main benefit of this enhanced sintering is a short densification time usu-

Table 1. Grain size values by FAST sintering nanocrystalline powders.

System	*Initial particle size* [nm]	*Powder preparation method*	*Final grain size* [nm]	*Grain size measurement method*	*Reference*
Ni	40	Plasma Synthesis	100	TEM	Kodash *et al.* [6]
Fe-Fe_3C	7-8	Mechanical Alloying	45	XRD (W-A)	Goodwin *et al.* [7]
Fe-Al	25	Mechanical Alloying	200-600	SEM	Venkataswamy *et al.* [8]
Cu-In-Ga-Se	N/A	Mechanical Alloying	62	XRD (W-A)*	Suryanarayana *et al.* [9]
TiN	70	Plasma process	90-100	XRD (W-A)	Groza *et al.*[10]
ZnO	20	Chemical Preparation	100	TEM	Gao *et al.* [11]
TiO_2	20	N/A	200	SEM	Lee *et al.* [12]
ZrO_2-Al_2O_3	N/A	Sol-gel (ZrO_2 matrix)	50	TEM	Yoshimura *et al.* [13]
Si_3N_4-TiN	5-20	Mechanical Milling	50	SEM	Yoshimura *et al.* [14]

* X-ray diffraction (Warren-Averbach)

Note: a direct comparison of the grain size values may be difficult due to differences in the reported measurement methods.

ally associated with minimal grain growth. Field sintering has been successfully applied for the densification of a variety of materials, electrically conductive, superconductors or insulators, monolithic and composite materials, regular size or nanocrystalline. Densities in excess of 99% have been achieved in sintering powders without any sintering additives. Selected examples of final grain sizes reached in field sintering of various nanopowders are shown in Table 1.

Nanocrystalline Ni powders (70 nm) were consolidated by FAST at 800K to > 91% density and a final grain size of 100 nm [6]. Our earlier studies on conventional Ni powders (~ 1 μm) showed a density of 93.7% at 0.65 T_{mp} (1123K) by PAS. For comparison, calculations for coarse Ni powders consolidated under the same temperature and pressure conditions, but without the electrical field, yielded a density value of only 81%.

Field sintering for 3 minutes at 725K of mechanosynthesized Fe-85%Fe_3C achieved 99% density with a final grain size of 45 nm [7]. This is to be compared to HIP densification of the same powders at 1025K for 60 minutes, with the same density value but final grain size of 87 nm.

Kimura and Kobayashi fully sintered mechanically alloyed TiAl powders and retained nanosize grains by SPS at 1051-1312K under modest pressures (29-147 MPa) [15]. Similar to conventional sintering, they showed that the densification temperature inversely scaled with the applied pressure.

Copper indium diselenide ($CuInGaSe_2$) obtained by mechanical alloying of elemental powders was fully consolidated in 10 min at 1023K by SPS using a 50 MPa pressure application [9]. The grain size was 62 nm as compared to 50 nm by hot pressing using a 100 MPa pressure. Although both densification methods yielded cracked specimens, reduced cracking was observed in the field sintered specimen cooled at a slower cooling rate (< 40 K/min).

The 90 nm grain size in field sintered TiN to 97% density at 1473K compares well with 0.5-1 μm obtained by conventional sintering at 1773K of the same 70 nm initial TiN powders [10]. More importantly, this study indicated less dependence of FAST

sintering on initial powder agglomeration as compared to conventional sintering.

ZnO nanoceramics (20 nm) have been processed by SPS at 823K for 2 min to a final density of 98.5% and grain size of 100 nm [11]. Generally, it is difficult to sinter ZnO without pronounced grain growth. Although the electric current enhances grain boundary diffusion in a semiconducting material such as ZnO, a heating rate of 200 K/min used in SPS sintering enabled the retention of the final grain size below 100 nm. The favorable response of a higher heating rate in ZnO is related to a lower activation energy for grain growth (~54 kJ/mol above 773K) than for densification (272 kJ/mole at 873-973K) [11, 16].

A very homogeneous structure with a grain size less than 100 nm was obtained in 96% dense $BaTiO_3$ ceramics [17].

In sintering 20 nm TiO_2, Lee *et al.* achieved the smallest final grain size in a 99% dense part by SPS sintering (200 nm) [12]. For comparison, microwave sintering yielded a final grain size of 300 nm and conventional sintering 1-2 μm. Noteworthy is also the full anatase to rutile phase transformation by SPS at 873K for 5 min, whereas simple heating under the same conditions preserved the initial anatase structure.

Nanometer SiC powder doped with 2.04 wt% Al_4C_3 and 0.4 wt% B_4C was consolidated by the SPS sintering techinque to near full density at 1872K with heating rates in the range 100 to 400 K/min [18]. As opposed to other ceramic materials, such as Al_2O_3 or TiO_2, the grain size increased when using faster heating rates.

Mishra and Mukherjee consolidated pure α-Al_2O_3 (50 nm) to >98% density in less than 10 min at 1573 K. The final grain size was 0.7 μm [19]. The conventional sintering of such powders reaches a similar density at 1773K in 3 h. 250 ppm additions of MgO resulted in a final grain size of 500 nm by field sintering at 1673K for 10 min. This work showed the favorable effect of multiple (i. e., repeated, see Fig. 2b) pulsing in PAS on alumina powder densification.

Dense ZrO_2/Al_2O_3 nanocomposites were processed by SPS starting from sol-gel prepared powders [13]. The final density was 97% with a grain size of ZrO_2 matrix of 50 nm when sintered at 1373K. The retaining of a nanometer microstructure was attributed to the rapid heating rates used (up to 200 K/min) and the effect of the Al_2O_3 as a grain growth inhibitor. For comparison, monolithic ZrO_2 had a grain size of 90 nm under the same sintering conditions.

The authors reported improved mechanical properties and low temperature plasticity, i. e., superplastic behavior at 1473K.

Yoshimura *et al.* synthesized nanosized Si_3N_4/TiN composites starting from mechanically milled nanopowders, with initial scale length of 5-20 nm [14]. The relative densities of the composites sintered at 1673K were above 99% with a final grain size of 50 nm for powders milled for 16h.

A notable feature of FAST consolidation is the enhancement of either phase transformations in single phase ceramics (e. g., anatase to rutile in TiO_2 [12]) or in reactions of single components to form compounds. An example for the latter is the Al_2TiO_5 formation form Al_2O_3 and TiO_2 components (Fig. 3) [20]. The time to densify the initial powders and form the final compound was shorter in SPS (10 min at 1473K) as compared to conventional sintering (2 h at 1573K). The total Al_2TiO_5 (tialite) amount increased faster when a field was applied as compared to conventional sintering. A similar enhanced phase transformation by field application was reported in Si_3N_4 ceramics [21]. A change in the defect structure by FAST sintering was observed in the 0.90 SnO_2 + 0.10 Sb_2O_3 ($Sn_{0.82}Sb_{0.18}O_2$) solid solution [22]. This change was related to an accelerated filling of the octahedral vacancies between the O^{2-} anions vacancies Sn^{4+} cations in the rutile structure of SnO_2-based solution. As seen in Table 2, the conventional sintering of $Sn_{0.82}Sb_{0.16}O_2$ ceramic is difficult due to the low diffusivity and no additives. FAST sintering of the same composition enabled a higher density value (92.4%).

Table 2. Comparison of Conventional and FAST Sintering of $Sn_{0.82}Sb_{0.18}O_2$.

Sintering	*Sintering parameters*	*Final Density,* %	*Grain Size,* μm	*Variation of Unit Cell Volume*, %
Conventional	1273K – 3h	61.3	N/A	0
FAST	1163K – 10min	92.4	<< 1	1.03

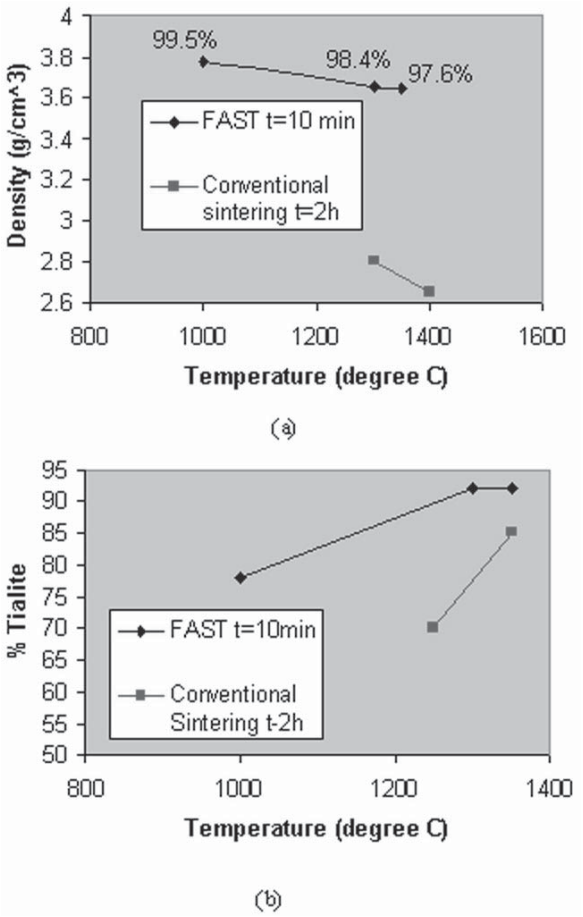

Fig. 3. Density of Al_2O_3-TiO_2 sample as a function of temperature (top). Reaction yield of FAST and conventional sintered Al_2TiO_5 (tialite) (bottom) [32].

3. DISCUSSION.

The exact mechanism of the enhanced FAST densification is not yet fully known. However, it is assumed that the pulsed electrical current creates favourable conditions for the removal of impurities and activation of powder particle surfaces for the subsequent particle-to-particle bonding [23]. The principle of FAST is based on the application of an AC+DC current through and around the specimen. Conduction along the die is important but it represents basically ohmic heating. Conduction through the specimen is more complex. When an electric current is conducted through a collection of particles, breakdown or tunneling of surface films, arcing, and constriction resistance phenomena may occur in the vicinity of contact areas [24].

The electrical breakdown is the back discharge in the surrounding gap between particles manifested by the presence of an arc. Recently, sparking has been observed by microscope in a copper powder compact [25], although under currents that are larger than the typical currents in FAST. The type of breakdown depends on the relative size between the gap and the mean free path of the gas, λ. If the gap d is such that $d<\lambda$ then vacuum breakdown occurs. For vacuum breakdown, the criterion of formation is independent of the gap d. If $d>\lambda$ then gas breakdown occurs. For instance, for atmospheric pressure and air breakdown occurs at V=340 Volts and d~8.6 μm. This is too high for arcing to occur in FAST, but it is possible that the high temperature of the contact may further decrease the critical conditions for discharge. An important phenomenon associated with arcing is material transfer, which results in a physical mechanism for charge transport along the gap. This is accomplished by vaporization of the surface of the material. This vapor can lead to intermittent plasma formation. It is conceivable that some surface cleaning from oxides and impurities take place during this process. Such arcing or electrical discharge phenomena at particle-to-particle contacts may be responsible for adsorbate elimination or surface "cleaning", thus enabling enhanced particle bonding during early sintering stages. This activation may explain the high densities obtained in ceramics without additives and direct grain-to-grain contact at atom scale observed by high resolution electron microscopy in FAST sintered materials (Fig. 4) [26, 27]. In additive-free AlN, the initial 5 nm shell of Al_2O_3 [28] on the AlN particle surface was redistributed into concentrated Al_2O_3 pockets (Fig. 4a). This redistribution may be a result of surface oxide vaporization. When the current is high, vapor is violently produced from the surface together with fine liquid droplets from the contact. An estimate of the maximum possible evaporation rate is given by:

$$\omega = \frac{440}{\rho_s J}\sqrt{\frac{M}{T}}(p - p_1), \qquad (1)$$

where ρ_S is the density of the material, J is the accommodated current density (A/m^2), M is the atomic weight, T is the temperature, p is the saturation pressure of the metal vapor and p_1 is the actual vapor pressure [29]. Typical values for ω are of the order of 10^{-11} m^3/coulomb. Generally, these vapors and micro-discharges at the powder particle contact points during the pulsed discharge step (current density above 100 A/cm^2) can lead to plasma formation. Our modeling studies of plasma as a continuum (fluid model of sheath) indicate that a low temperature gas plasma state (plasma density

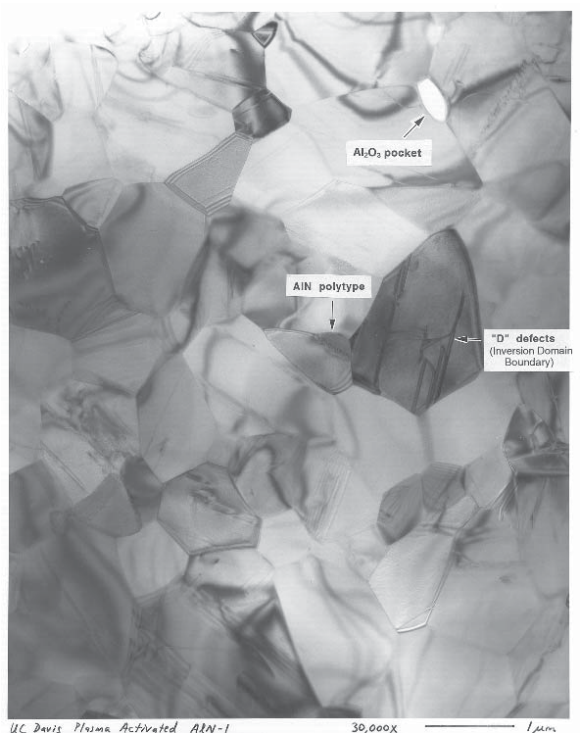

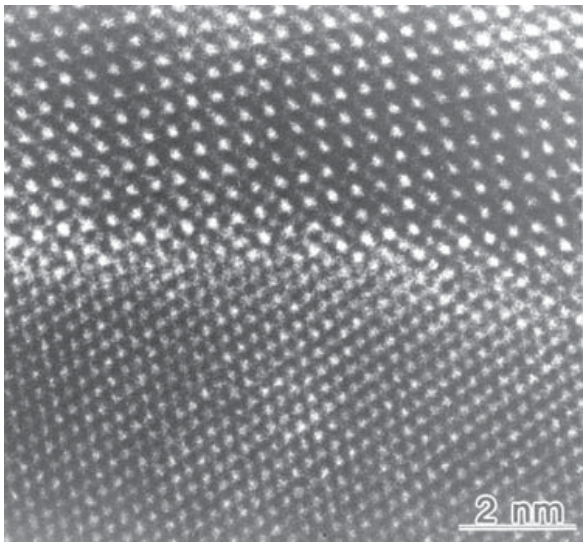

Fig. 4. Regular (left) and high resolution TEM (right) of field sintered AlN.

of about $10^{13}/cm^3$) may be created [27]. However, the experimental verification of this plasma or other type of surface effects due to electric field activation has not yet been unambiguously established. The cleaning ability of the applied current was at least partially shown by the lack of a desorption process in measuring the electrical conductivity variation with temperature in FAST sintered SnO_2 specimens. Such a desorption (i. e., adsorbates still present) was noticed at 600K in same materials by conventional sintering [22].

Electrical resistance due to the constriction offered by the conducting spots depends on: (a) the resistivity ρ of the base material, (b) the size of conducting spots that concentrate the equipotential surfaces toward the contact, (c) the number and the near-neighbor distance of the conducting spots due to the distortion of the electric field caused by neighboring spots when they are close to each other. A simple estimate of the contact resistance, R, is $R=\rho/(2a)$, where a is the contact size [29]. As the contact area decreases, although the current $I = \int \bar{J} d\vec{A}$ is very small, the current density becomes very high. When the size of the contact 'neck' decreases, we move into two different length scales. When the scattering length L of the charges becomes comparable with the length scale of the contact, the so-called Knudsen effect occurs [30]. The Knudsen number $K=L/a$ is used in analogy with the similar problem of the flow of low pressure gas through a small hole into vacuum. Under such conditions the contact resistance can be written as:

$$R = \frac{\rho}{2a} + \frac{4}{3}\frac{K}{\pi a}\left(\frac{L}{a}\right), \qquad (2)$$

where the second term is termed the Knudsen resistance. The key implication of the concept of Knudsen resistance is the absence of significant scattering around the contact, which will accelerate the charge carriers significantly through the constriction. For typical conductive powders the scattering length is on the order of 10 nm. For the Knudsen number to be important the contact size must be of the order of 20 nm. This is possible only in the early stages of the process and provided that low external pressure is applied. The presence of Knudsen resistance is often related to very high electromigration action in the contact due to the strong effect of the extreme current intensity at the contact. In fact, in this case and for conventional electrical contacts, it is claimed that such contact is "self-cleaning" because impurities will be driven rapidly away from the contact under the action of electron wind. In general, sintering of nanosize powders is faster than micron-scale powders. However, the small ratio of volume to surface area implies

that surface impurities may dominate the response of the material and in traditional sintering this may adversely affect the sintering rate. Any "contact" cleaning action on the interparticle contacts, such as by field application, will lead to accelerated sintering and significant advantage in properties.

An important issue in FAST is the uniformity of the electrical current. In the early stages when the relative density of the powder is small, the size of the interparticle contacts varies significantly. As a result, under certain conditions, concentration of the current along discrete favorable paths is observed. If the resulting localized heat can not be effectively transferred away, then a further reduction of the local resistance occurs with catastrophic effect (localized melting). When the size of the powders is very small (sub-micron) then the efficiency in powder packing is also small and the non-uniformity of conducting paths is significant. On the other hand, the small size of the powder promotes heat conduction.

This unfavorable localization of the electric current in the compact is alleviated effectively with the application of pressure when the powder size is relatively large. Pressure role in electric conduction manifests in two ways: (1) the flattening of the contacts results in a decrease in resistance by alleviating the constriction effect, and (2) the deformation of the particle-to-particle contacts causes the surface film to "rupture" with a attendant increase of conducting spots. Both these effects should reduce the macroscopic resistivity and the corresponding ohmic heat generation. Another related effect is the increase of the coordination number by the application of pressure. The coordination number increases from Z=5..7 in tapped powders to 12..14 upon pressure application. The increase of coordination number implies that new conducting contacts are forming where previously powder particles where separated by a gap. In this way the spatial density of current paths in the compact increases, which in turn provides a more uniform transmission of current. Possible generation of arcs around the interparticle contacts may contribute to further heat generation. Although this heat generation is highly localized, the typically small radius of the powder particles results in a near uniform distribution of temperature.

As shown above, the enhanced densification in field sintering is most noticeable at lower temperatures when the discharge effects are operational. The highest temperatures achieved in the necks provide the highest diffusion rates and thus enhanced

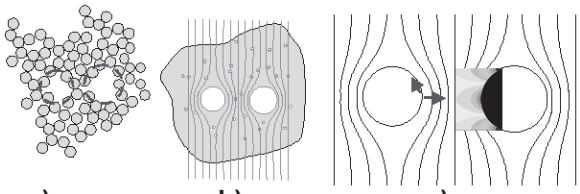

Fig. 5. (a) Agglomerated powder, (b) bimodal pore distribution as a result of inefficient packing of agglomerates, and (c) electric field amplification at the root of the pores resulting in temperature gradients, which in turn produce *vacancy gradient* (arrows) and mass transport in the opposite sense.

matter transport towards the neck area. This is the area in which most of the matter transport is required for sintering. Therefore, field application intensifies the sintering rate. Beyond the electrical discharge stage, the sintering parameters in FAST have a similar effect as in conventional pressure sintering. Diffusional processes and plastic flow are the main contributors to the densification. Diffusion studies indicate the extensive contribution of an applied electrical current (e.g., electromigration) in all sintering stages. In the initial sintering stages, the local discharge processes, which disrupt the surface layers induce various types of defects that enhance surface and grain boundary diffusion. This way, both densification and grain growth are accelerated. Basic studies showed that the field application is likely to enhance grain boundary velocity due to impurity elimination. In intermediate and final stages of sintering, a charge gradient is developed in the vicinity of pores with different sizes. Similar to initial particle contacts, the electrical field increases as the concentration of equipotential lines increases in late sintering stages (Fig. 5). As a result, electrical current density is larger next to large pores than small pores. This creates a temperature gradient, i. e., the temperature is higher next to large pores than next to small pores. Raichenko calculated the temperature gradient, ∇T, which develops in the vicinity of these pores under pulsed field application [31]:

$$\nabla T \approx \frac{1}{R}\sqrt{\frac{\sigma_0}{2C_M}\cdot\frac{T_0E_0^2\Delta\tau}{n}}, \qquad (3)$$

where R is the pore radius, σ_0 – electrical conductivity, C_M – specific heat, T_0 – initial temperature, E_0 – intensity of electric field, $\Delta\tau$ – time of electric field

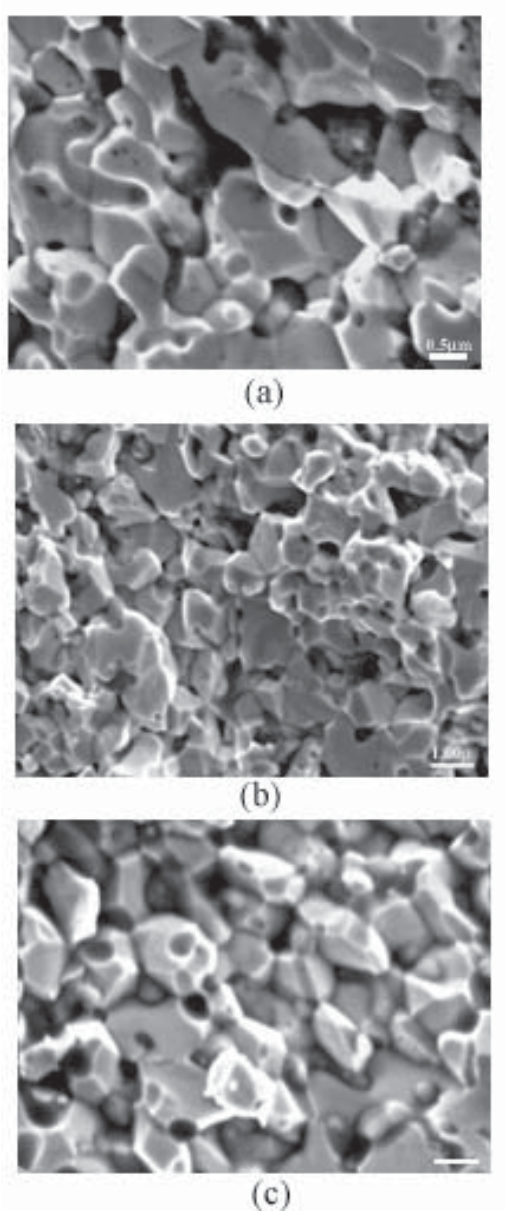

Fig. 6. SEM micrographs of $MoSi_2$ samples, FAST sinterd at 1473K, with heating rates of: a) 50 K/min, b) 250 K/min, c) 700 K/min.

effect, n – number of electrical impulses. In turn, this temperature gradient generates a vacancy gradient, ∇C_v, or more vacancies are created in the vicinity of large pores. The vacancy flow, J, is given by [31]:

$$J = D_v (k_T/T\nabla T - \nabla C_v), \quad (4)$$

where D_v – is the diffusion coefficient of vacancies and k_T is the thermal diffusivity. Therefore, vacancy diffusion occurs from large pores towards the small pore, resulting finally in the shrinkage of large pores. This is opposite to conventional sintering in which a large pore grows at the expense of small pores. Our previous experimental studies indeed indicated an advanced pore closure in the FAST sintered powders [32]. Large pores with convex curvatures were seen in $MoSi_2$ in late sintering stages, indicative of the pore shrinkage (i. e. moving towards the center of curvature) (Fig 6).

The success in nanopowder consolidation is intimately related to the control of the densification-coarsening competition. Both sintering and coarsening driving forces are larger in nanoparticles than in their coarse counterparts. Similar to coarse grained materials, the coarsening kinetics are given by [33]:

$$G^2 - G_0^2 = 2\alpha M_b \gamma_{gb} t, \quad (5)$$

where G is the grain size, G_0 the initial grain size, α is a constant, M_b is the grain boundary mobility, γ_{gb} the grain boundary energy and t is time. Generally, a rapid reduction in porosity will also result in coarsening. Exaggerated grain growth when the porosity becomes of closed type (i. e., at densities > 90%) has been shown in the sintering of both metal and ceramic nanopowders [34]. A similar trend was observed in field sintering. Table 1 shows that the grain size of some FAST sintered samples exceeds the 100 nm limit. However, FAST offers means to retain the fine grain size during both early and late sintering stages. These include a high heating rate and shortest time at high temperatures, respectively. Pressure application also may control the breaking of powder agglomerates and minimize coarsening by particle re-arrangement. In addition, the applied pressure plays a significant role in the uniformity of the current flow. The application of pressure in FAST has been shown to enhance densification in late sintering stages in the same way as in conventional sintering (by plastic yielding or diffusional creep) [10].

Basic studies of the heating rate effects (up to 700 K/min) in FAST sintering were quantified for α-Al_2O_3 and $MoSi_2$ powders [32]. Generally, fast heating rates are used in sintering to favor densification over grain growth in coarsening sensitive systems [e. g., 35]. These systems are characterized by a higher activation energy for diffusion than for grain growth, such as Al_2O_3 and ZnO [16, 32]. A high heating rate will not allow surface diffusion to coarsen the structure at low temperatures. Instead, the sintering powders are quickly taken to high temperatures where densification becomes predominant. The effect of FAST heating rate on sintering Al_2O_3 at 1473K is shown in Fig. 7. The experimental

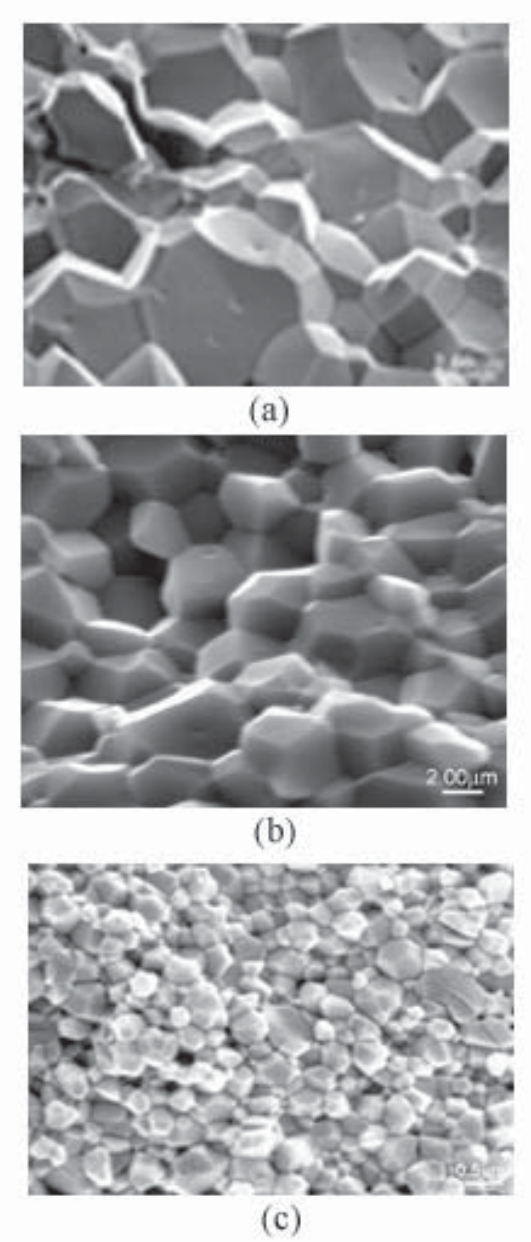

Fig. 7. SEM micrographs of Al_2O_3 specimens FAST sinterd at 1473K for 2 minutes with heating rates of: a) 50 K/min, b) 250 K/min, c) 700 K/min.

grain size values follow the grain growth equation developed by Chou *et al.* [36]:

$$G^m(T) = G_0^m + \frac{g_0}{\alpha}\int_{T_0}^{T} \exp\left(-\frac{Q_g}{kT}\right)dT, \qquad (6)$$

where G_0 is the starting grain size at time $t = t_0$, m is a constant, g_0 is a material constant, α is the constant heating rate, Q_g is the activation energy for grain growth, k is the Boltzmann constant, and T is the absolute temperature. A similar behavior was recently reported in field sintering of Al_2O_3 by Nygren's group [21]. As expected from above equation, temperature plays the most important role in alumina coarsening. They found a grain growth rate three times faster at 1573K than at 1473K. In contrast, no dependence of grain size on heating rates was observed in $MoSi_2$ (Fig. 6) [32]. Generally, lowering the sintering temperature can help maintaining a fine grain size of the final material since the grain boundary migration, which promotes grain growth is temperature dependent.

5. CONCLUSIONS

A variety of conductive, non-conductive and semiconductor nanosize powders were sintered to high densities by field activated sintering. The rapid rate of densification, no need for preliminary powder preparation steps such as cold compaction, additive use and debinding, short time at high temperatures are some densification characteristics that may make the FAST process economically competitive. This is especially true for difficult to cold press, oxygen-sensitive, and metastable materials such as nanocrystalline powders. Grain growth may be controlled by reducing time and temperature of sintering and, for coarsening sensitive materials, by applying high heating rates.

The densification phenomena specific to electrical field applications are electrical discharges, breakdown, arcing, constriction resistance, and vacancy-current interaction. The temperature, time and pressure application have similar effects as in conventional sintering.

REFERENCES

[1] G. F. Taylor, *US Patent* No. 1,896,854, Feb 7,1933.
[2] F. V. Lenel // *JOM* **7** (1955) 158.
[3] J. R. Groza, In: *ASM Materials Handbook*, vol. **7** (ASM International, Materials Park, Ohio, 1998) p. 583.
[4] *High pressure field sintering apparatus* (UC Davis, 2002).
[5] K. Okazaki // *Rev. Particulate Mater.* **2** (1994) 215.
[6] V. Y. Kodash, J. R. Groza, R. L. Dowding and K. Cho, *FAST sintering of nanocrystalline Ni powders*, to be submitted.
[7] T. J. Goodwin, S. H. Yoo, P. Matteazzi and J. R. Groza // *Nanostr. Mater.* **8** (1997) 559.

[8] M. A. Venkataswamy, J. A. Schneider, J. R. Groza, A. K. Mukherjee, K. Yamazaki and K. Shoda // *Mat. Sci. Eng.* A207(1996) 153.
[9] C. Suryanarayana, S. H. Yoo and J. R. Groza // *J. Mater. Sci. Lett.* **20** (2001) 2179.
[10] J. R. Groza, J. Curtis and M. Kraemer // *J. Am. Ceram. Soc.* **83** (2000) 1281.
11. L. Gao, Q. Li, W. Luan, H. Kawaoka, T. Sekino and K. Niihara // *J. Am. Ceram. Soc.* **85** (2002) 1016.
[12] Y. I. Lee, J-H. Lee, S-H. Hong and D-Y. Kim // *Mat. Res. Bull.* **38** (2003) 925.
[13] M. Yoshimura, M. Sando, Y. H. Choa, T. Sekino and K. Niihara // *Key Eng. Mat.* **161-163** (1999) 423.
[14] M. Yoshimura, O. Komura and A. Yamakawa // *Scr. Mater.* **44** (2001) 1517.
[15] H. Kimura and S. Kobayashi // *J. Japan Inst. Met.* **58** (1994) 201.
[16] A. P. Hynes, R. H. Doremus and R. W. Siegel // *J. Am. Ceram. Soc.* **85** (2002) 1979.
[17] Z. Zhe, Arrhenius Laboratory, Stockholm University, Private Communication, 2002.
[18] Y. Zhou, K. Hirao, M. Toriyama and H. Tanaka // *J. Am. Ceram. Soc.* **83** (2000) 654.
[19] R. S. Mishra and A. K. Mukherjee // *Mat. Sci. Eng.* **A287** (2000) 178.
[20] L. A. Stanciu, J. R. Groza, V. Y. Kodash, M. Crisan and M. Zaharescu // *J. Am. Ceram. Soc.* **84** (2001) 983.
[21] Z. Shen, M. Johnson and M. Nygren // *J. Am. Ceram. Soc.* **85** (2002) 1921.
[22] O. Scarlat, S. Mihaiu, Gh. Aldica, M. Zaharescu and J. R. Groza // *J. Am. Ceram. Soc.* **86** (2003) 893.
[23] J. R. Groza and A. Zavaliangos // *Mat. Sci. Eng. A* **287** (2000) 171.
[24] A. Zavaliangos, *A first order model for resistivity sintering*, (in preparation).
[25] G. Yanagisawa, H. Kuramoto, K. Matsugi and T. Hatayama, In: Proceedings of Nedo Conf., Japan (1999) p. 127-133.
[26] S. H. Risbud, J. R. Groza and M. J. Kim // *Phil. Mag.B* **69** (1994) 525.
[27] J.A. Schneider, J.R. Groza and M. Garcia // *J. Mater.Res.* **16** (2001) 286.
[28] J. H. Harris // *JOM* **50** (1998) 56.
[29] R. Holm, *Electric Contacts: Theory and Applications, 4th Ed.* (Springer-Verlag, New York, 1967).
[30] A.G.M. Jansen, F.M. Mueller and P. Wyder // *Science* **199** (1978) 1037.
[31] A. I. Raichenko, *Funadmental Porcesses in Powder Sintering* (Metallurgyia, Moscow, 1987).
[32] L. A. Stanciu, V. Y. Kodash and J. R. Groza // *Met. Mater. Trans.* **32A** (2001) 2633.
[33] T. R. Mallow and C. C. Koch // *Acta Mater.* **45** (1997) 2177.
[34] J. R.Groza, In: *Nanostructured Materials*, ed. by C. C. Koch (W. Andrew Publishing, Norwich, 2002).
[35] M. Harmer, W. W. Roberts and R. J. Brook // *Trans. J. Br. Ceram. Soc.* **78** (1979) 22.
[36] M. Y. Chu, M. N. Rahaman and L. C. DeJonghe // *J. Am. Ceram. Soc.* **74** (1991) 1217.